J Appl Electrochem (2012) 42:909–915
DOI 10.1007/s10800-012-0470-9

ORIGINAL PAPER

Electrochemical characteristics of nano-sized MoO_2/C composite anode materials for lithium-ion batteries

Woosuk Cho · Jun Ho Song · Jae-Hun Kim · Goojin Jeong · Eun Young Lee · Young-Jun Kim

Received: 23 May 2012 / Accepted: 31 July 2012 / Published online: 10 August 2012

Abstract A nano-sized MoO_2/C composite was synthesized using a spray pyrolysis technique, and investigated as an anode material for Li-ion batteries. Spherical MoO_2/C particles with the monoclinic phase were obtained without any impurities, and with a primary particle size in the range 30–50 nm. Structural variation of the prepared MoO_2/C during Li^+ insertion was examined by in situ X-ray diffraction and selected area electron diffraction analyses. The structural analysis results indicated that no conversion reaction was activated in the MoO_2/C composite. The electrochemical tests demonstrated that the rate-capability and capacity retention of the synthesized materials were improved significantly, which could be attributed to the effective carbon distribution and nano-sized primary particle resulting from the low-synthesis temperature. Therefore, control of the powder morphology and minimization of the primary particle size are found to be essential for achieving the enhanced electrochemical properties in MoO_2 anode materials.

Keywords Li-ion battery · Electrode · Molybdenum dioxide · Spray pyrolysis

1 Introduction

In recent years, lithium-ion batteries (LIB) have been used widely for power source of mobile information technology (IT) devices and the application fields of LIB can be extended to transportation applications such as electric vehicles (EVs) and hybrid electric vehicles (HEVs). For the successful launch of large-scale lithium-ion batteries in the transportation field, improvements are needed in terms of their energy and power density, and the safety of the batteries and packs must be guaranteed [1–3].

In many cases, anode materials can play the key role in the safety of a battery. The reaction potential of graphite, which is used commercially, is close to the reaction potential of Li metal anode, and thus, lithium metal dendrite can be formed on the surface of the graphite in the overcharged state or under abuse conditions [4]. This safety issue can be solved using alternative anode materials such as transition metal oxides with higher operating voltage than that of the graphite anode [5–7]. Because these metal oxides undergo redox reactions above the potential of Li metal formation, the new anode systems are able to obtain the innovative safety of lithium-ion batteries [8]. The first transition metal oxide to be commercialized as an anode material was spinel-type lithium titanate, $Li_4Ti_5O_{12}$. However, this material has a low-energy density compared to the graphite anode [8, 9], and many researchers have investigated other transition metal oxides that show high capacities such as MoO_2, NiO, and TiO_2 [5–7, 10–13].

Among such oxide-based anode materials, molybdenum dioxide (MoO_2) is a promising material because of its good electrical conductivity [14–16]. MoO_2 belongs to the space group of $P2_1/c$, which is constructed of a framework and a tunnel structure parts. The framework possesses rutile-type structure, which consists of MoO_6 octahedrons linkage as shown in Fig. 1. Tunnels are located inside framework structure, or one dimensional channel along the a-axis, where Li-ions can be inserted/extracted reversibly.

The phase transition from the monoclinic M1 ($P2_1/c$) phase to the M2 phase via the orthorhombic O phase

W. Cho · J. H. Song · J.-H. Kim · G. Jeong · E. Y. Lee · Y.-J. Kim (✉)
Advanced Batteries Research Center, Korea Electronics Technology Institute, #68 Yatap-dong, Bundang-gu, Seongnam-si, Gyeonggi-do 463-816, Korea
e-mail: yjkim@keti.re.kr

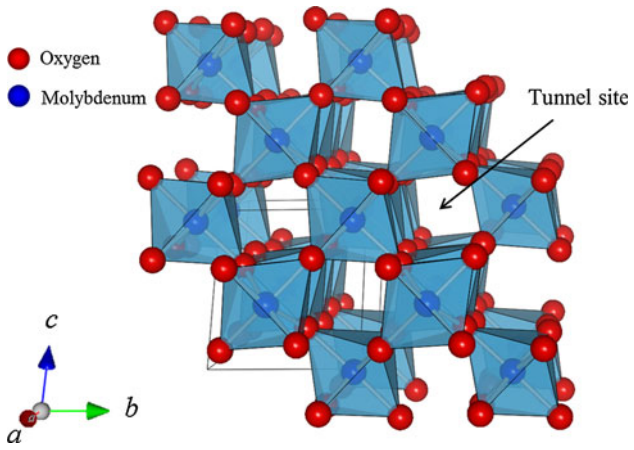

Fig. 1 Crystal structure of the rutile-type MoO_2; Li-ions can be inserted in tunnel

(*Pnnm*) occurs with a volume change of 11 % for the change from MoO_2 to $LiMoO_2$ (insertion of one Li on per formula unit), which induces material degradation of the MoO_2 negative electrode [17]. Normally, MoO_2 is prepared by the reduction of MoO_3 under a hydrogen atmosphere at a high temperature, which results in large particle sizes [10, 18, 19]. A large particle size can lead to negative effects such as a large volume change of the material. It is known that the large surface area and short length of ion diffusion pathway of nano-sized materials are beneficial in terms of the electrochemical properties of electrode materials [13]. Therefore, the preparation of nano-sized or nano-structured materials would be an effective way to design electrode materials.

In this study, a nano-structured spherical MoO_2 material with a primary particle size of 30–50 nm was synthesized by a spray pyrolysis technique which is a very competitive method for the preparation of nano-sized and nano-structured material [9, 12, 20, 21]. Furthermore, the synthesis of the MoO_2/C composite was achieved at a relatively low temperature of 650 °C by adding sucrose as a carbon source additive. The structure, morphology, and electrochemical properties of the nano-sized MoO_2/C composite were investigated using various analytical techniques.

2 Experimental

The spray pyrolysis technique is well known for the preparation of nano-sized or nano-structured materials [9], and a schematic diagram of the system was presented in our previous work [21]. Hexaammonium heptamolybdate tetrahydrate ($(NH_4)_6Mo_7O_{24}{\cdot}4H_2O$) was used as the starting material, and sucrose ($C_{12}H_{22}O_{11}$) was used as the reducing agent and carbon source. The mixed solution was poured directly into an ultrasonic nebulizer for the creation of minute droplets. The bubbled precursor was carried into a vertical tube furnace and heat-treated under a flow of the mixture gas Ar/H_2 (95/5) at a temperature of 650 °C. The heat-treatment temperature was optimized in advance through comparisons of the crystal phase and particle size. Commercial MoO_2 powders (Sigma-Aldrich) were used as reference materials for comparison.

X-ray diffraction (XRD, both powder and in situ) patterns were obtained using an Empyrean diffractometer (PANalytical) equipped with monochromated Cu Kα radiation ($\lambda = 1.54056$ Å). The in situ XRD was performed using a lab-made in situ cell. The powder morphology was characterized by field-emission scanning electron microscopy (FESEM, JEOL JSM-7000F) with energy dispersive spectroscopy (EDS) mapping. Selected area electron diffraction (SAED) patterns were acquired through high-resolution transmission electron microscopy (HR-TEM, JEOL JEM-2100F). The amount of carbon in the MoO_2/C composite was measured by CHNSO elemental analysis (ECS 4010, Costech Inc.). Differential scanning calorimetry (DSC, Model Star system, Mettler Toledo) was performed to investigate the thermal characteristics of the lithiated electrodes. The heating rate and temperature range of the test were 5 °C min^{-1} and 25–400 °C, respectively.

The electrodes were prepared by coating copper foil or mesh with slurries containing active material powders (80 wt%), carbon black (Super P, 10 wt%), and polyvinylidene fluoride (PVDF) dissolved in *n*-methyl-2-pyrrolidone (NMP). After coating, the electrodes were pressed and dried for 12 h at 120 °C. Coin-type cells (CR 2032) were assembled in a dry room with the dew point controlled to less than −45 °C. The cells consisted of the MoO_2 working electrode, a Li-metal foil counter electrode, a porous polyethylene membrane separator, and 1 M $LiPF_6$ dissolved in ethylene carbonate (EC) and dimethyl carbonate (DMC) (1:2 in volume ratio) as the electrolyte (Panax Etec). The discharge (lithiation)–charge (delithiation) experiments were performed galvanostatically at a constant current between 0.1 and 5 C using a TOSCAT-3100U cycler (Toyo system Co.) at room temperature. Cyclic voltammetry was carried out using a Solartron 1287 potentiostat with a three-electrode glass cell setup, where Li-metal foil was used as the counter and reference electrode.

3 Results and discussion

The powder XRD patterns for the MoO_2/C composites prepared by spray pyrolysis and the commercial powder are shown in Fig. 2, together with a simulated XRD pattern taken from the inorganic crystal structure database (ICSD #23722) [22]. For the sample prepared at 600 °C, diffraction peaks for both MoO_2 and MoO_3 are observed. When

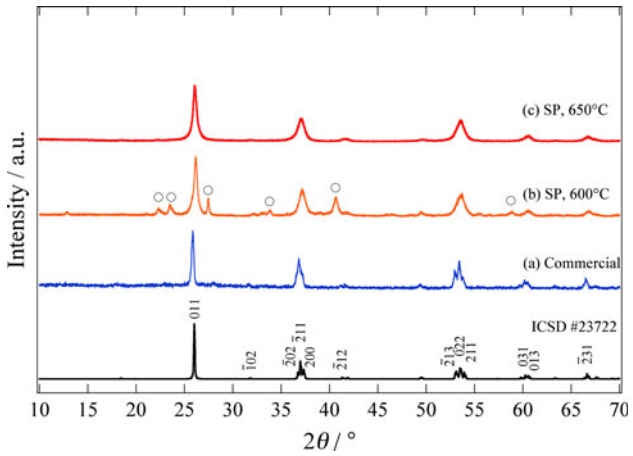

Fig. 2 Powder X-ray diffraction patterns of prepared and commercial powders; **a** commercial MoO_2 powder, **b** prepared at 600 °C, and **c** 650 °C. *Circle* marks the peaks for MoO_3 phase

the synthesis temperature is increased up to 650 °C, the single phase MoO_2 diffraction pattern is observed within the detection limit of XRD, which is in good accordance with a rutile-crystal structure (space group $P2_1/c$). In general, MoO_2 powders are prepared by the reduction of MoO_3 at a high temperature of around 800 °C. In this study, full conversion into MoO_2 was achieved at a relatively low temperature of 650 °C by 5 % hydrogen and ammonia gas decomposed from starting material, $(NH_4)_6Mo_7O_{24}{\cdot}4H_2O$, and sucrose as reducing agents. It is found that the diffraction peaks are broadened, indicating that the crystallinity and/or particle size are different from those of commercial MoO_2 powders. The corresponding full width at half maximum (FWHM) value for 011 peak was calculated to be 0.748. From the FWHM value, the crystalline size of the synthesized material was estimated to be 15 nm using Debye–Scherrer formula, which indicates that nanocrystalline characteristic of the particle is expected.

FESEM images of the MoO_2/C composite are presented in Fig. 3. It is observed that the particles have a spherical shape with a primary particle size in the range 30–50 nm. Figure 4 shows the EDS mapping results, demonstrating the presence of Mo, O, and C in the powders. It is detected that the carbon is uniformly distributed over the entire range. The CHNSO elemental analysis shows that the quantitative amount of carbon is 2.8 wt%. In the XRD pattern, there is no visible reflection of carbon, which indicates that the carbon in the MoO_2/C composite exists as an amorphous phase. It is worth noting that the sucrose material plays a bifunctional role, acting simultaneously as both the reducing agent and the carbon source in the composite. On the basis of the above results, it was confirmed that the spherical MoO_2/C nano-sized composite was prepared successfully by the spray pyrolysis method.

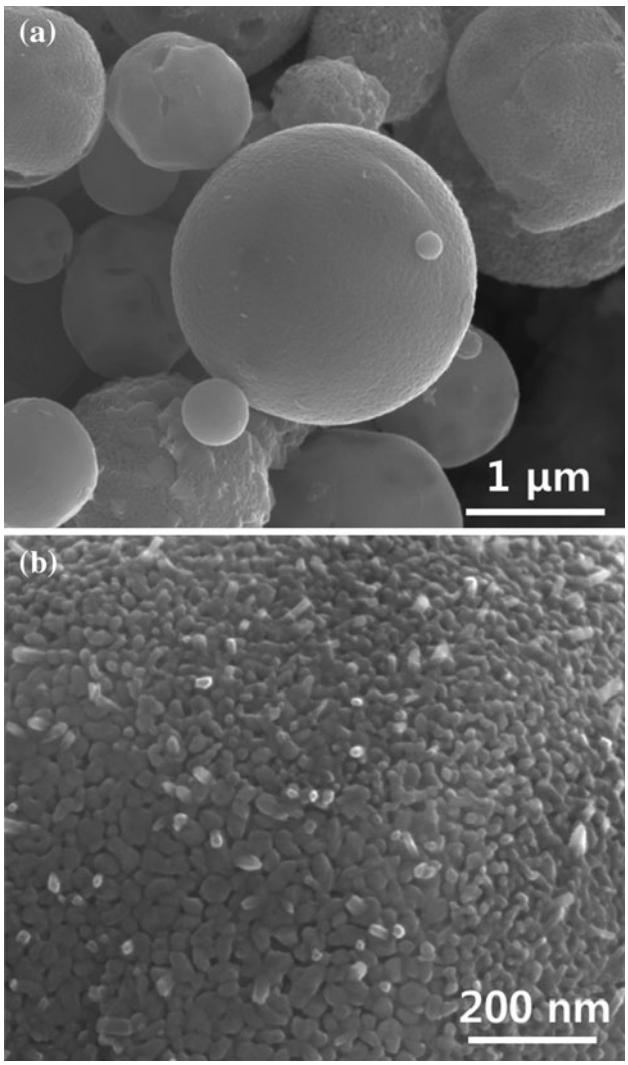

Fig. 3 FESEM images of nano-sized MoO_2/C composite **a** at low magnification, and **b** at high magnification

In general, the electrochemical reactions of transition metal oxides as anodes with Li can be classified into two groups: (i) the insertion reaction of Li into the crystal structure of the electrode material, and (ii) the conversion reaction of complete decomposition to Li_2O and the inactive transition metal oxide [3]. In the case of MoO_2, it has been reported that Li^+ insertion proceeds through both steps, i.e., (i) the insertion reaction from the initial state to approximately 0.8 V, and (ii) the decomposition (conversion) reaction at a deeply charged state to about 0 V [14, 23]. This reaction can be expressed as follows:

$$\text{Insertion}: \ MoO_2 + Li^+ + e^- \rightarrow LiMoO_2 \ (1 \text{ electron}) \quad (1)$$

$$\text{Conversion}: \ LiMoO_2 + 3Li^+ + 3e^- \rightarrow Mo + 4Li_2O \ (3 \text{ electrons}) \quad (2)$$

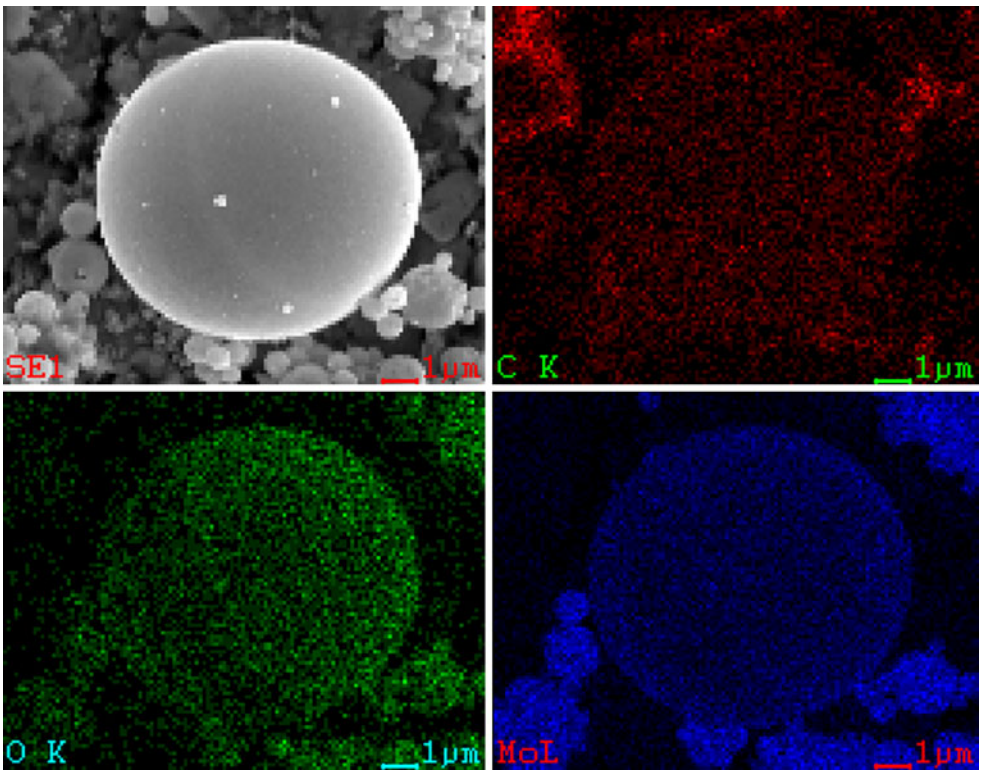

Fig. 4 EDS element mapping results for nano-sized MoO_2/C composite

Here, the conversion reaction is generally activated at elevated temperature due to the kinetic barrier of MoO_2 [23]. In some cases, for MoO_2 with a mesoporous structure or nanostructure, the conversion reaction is activated at room temperature; this may result from the enhanced reaction kinetics due to the short Li-ion pathways [10, 16, 24–27].

Cyclic voltammetry was carried out to investigate the reaction mechanism of the synthesized MoO_2/C composite. Figure 5 shows cycle voltammograms of the MoO_2/C composite electrode measured in the voltage range 0.02–3.0 V with a scan rate of 0.5 mV s^{-1}. Two pairs of cathodic and anodic peaks at 1.1/1.5 and 1.3/1.8 V are clearly observed in the first cycle. Two cathodic peaks are related to the phase transition from monoclinic to orthorhombic during Li^+ insertion [17]. From the second cycle, the cathodic peak positions are shifted to 1.2 and 1.5 V, respectively. This indicates that irreversible reactions occur for the initial Li^+ insertion and then, no visible change is observed in the subsequent cycles.

For a clear understanding of the reaction, a detailed investigation of the structural variation during cycling was performed using in situ XRD measurement. Figure 6 shows the in situ XRD patterns in the voltage range 3.0–0.02 V during Li^+ insertion. In the initial state, the phase of MoO_2 is a monoclinic M1 phase ($P2_1/c$). Upon further Li^+ insertion, the phase transforms into an orthorhombic O

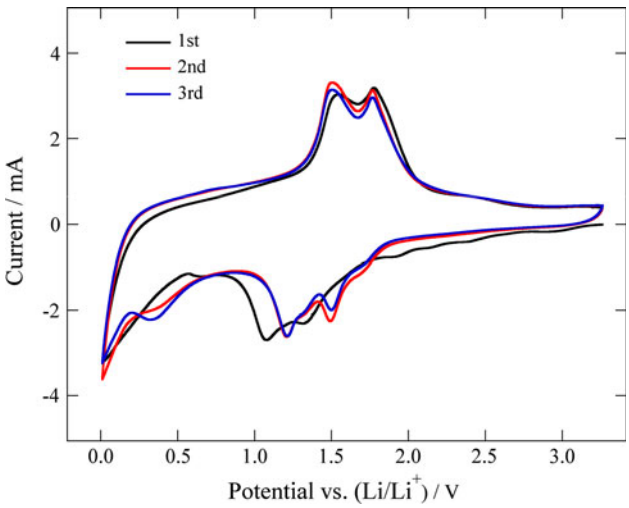

Fig. 5 Cyclic voltammograms of nano-sized MoO_2/C composite at a scan rate of 0.5 mV s^{-1}

phase (*Pnnm*), and the final phase becomes a monoclinic M2 phase ($P2_1/c$) below 0.8 V. This structural variation is in good accordance with the results reported by Dahn and McKinnon [17]. As the voltage decreases to 0.02 V, the M2 phase is maintained and no additional peak is detected, which indicates that no phase transition occurs below 0.8 V. In general, a conversion reaction undergoes the formation of metal element and Li_2O in nanosizes through

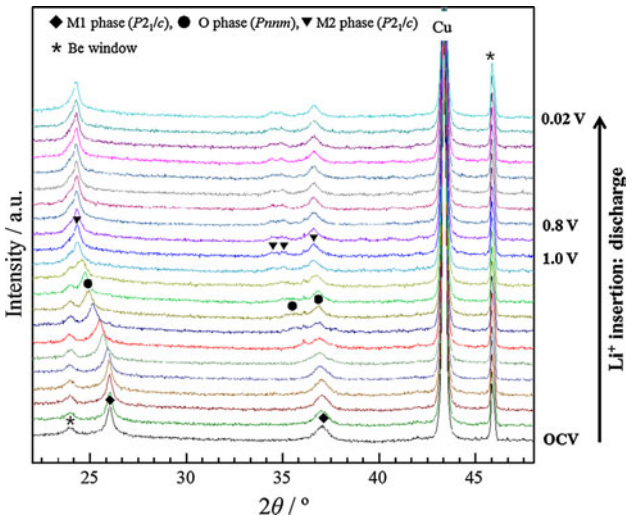

Fig. 6 In situ XRD patterns of nano-sized MoO_2/C composite during electrochemical Li^+ insertion

the electrochemical grinding phenomenon [3]. In the MoO_2 nanoparticles in this study, the conversion reaction was not observed in the in situ XRD patterns; for further confirmation, SAED patterns were obtained through HRTEM analysis. Figure 7 shows the SAED patterns of pristine and discharged MoO_2. The patterns of the pristine MoO_2 can be attributed to the M1 phase (Fig. 7a), and those of MoO_2 discharged to 0.8 and 0.02 V (Fig. 7b, c, respectively) are assigned to the M2 phase. In the pattern of the sample discharged to 0.02 V, no additional diffraction pattern related to Mo and Li_2O is found, indicating that the conversion reaction is not activated in the MoO_2/C composite.

Galvanostatic discharge–charge cycling was performed in the potential range 3.0–0.8 V, which is the region of the as-known insertion/extraction reaction. Voltage profiles of the nano-sized MoO_2/C composite electrode are shown in Fig. 8. The first discharge and charge capacities are about 270 and 225 mAh g^{-1}, respectively, with an initial coulombic efficiency of 84 %. The reversible discharge capacity of the MoO_2/C composite is higher than the theoretical capacity (209 mAh g^{-1}), which could be due to the nano-sized primary particles of MoO_2, which allow higher Li^+ occupancies of the near-surface environment [28]. The first discharge curve slopes gradually down from 1.7 to 1.2 V, which is a typical feature of nanomaterials, reported frequently in the literature [28, 29]. The irreversible capacity in the first cycle is possibly due to the decomposition of the electrolytes and formation of a solid electrolyte interphase, which might be generated on the large surface area of the nano-sized MoO_2 [28, 30]. The second discharge–charge curve exhibits two typical discharge plateaus at 1.55 and 1.25 V and two charge plateaus at 1.35 and 1.70 V, which is in good agreement with the CV results.

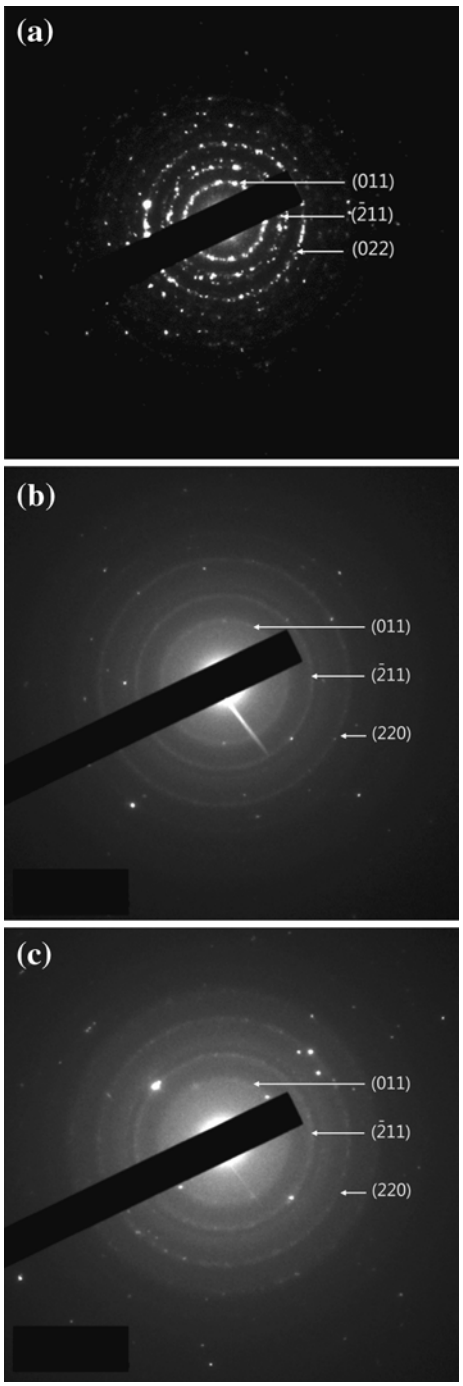

Fig. 7 SAED patterns of MoO_2 electrodes at various depth of discharge; **a** pristine, **b** 0.8 V, and **c** 0.02 V

The rate characteristics of the MoO_2/C material are plotted as a function of the C-rate in Fig. 9. Commercial MoO_2 powders were used for comparison purposes. The discharge capacities were normalized with respect to the C-rate of the same electrode at the slowest rate of 0.1 C. The nano-sized MoO_2/C shows an improved rate-capability compared with the commercial MoO_2. The capacity of the nano-sized MoO_2/C composite electrode at 0.1 C is

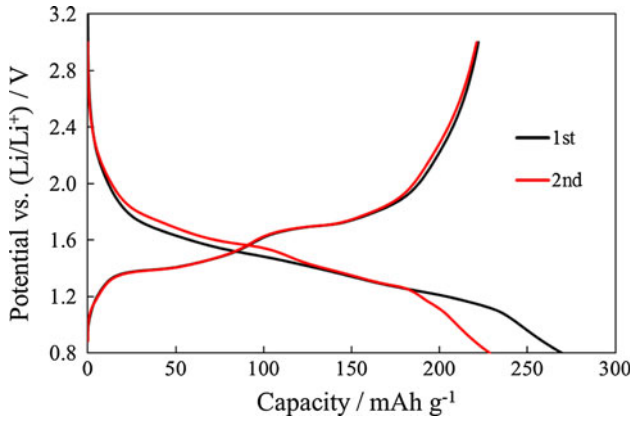

Fig. 8 Voltage profiles of nano-sized MoO_2/C composite

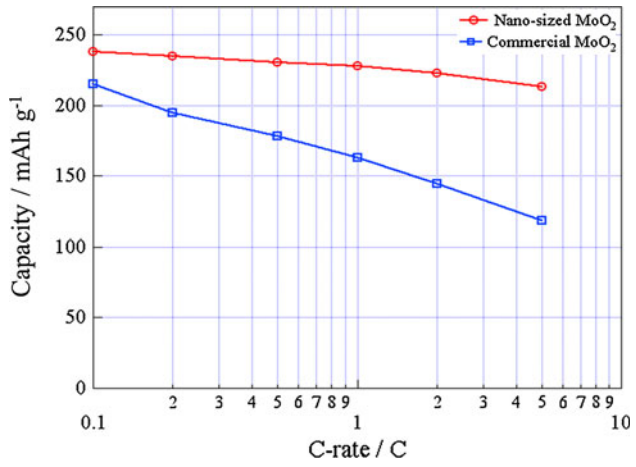

Fig. 9 Rate-capability for nano-sized MoO_2/C composite and commercial MoO_2 (particle size: 200–400 nm) at various C-rates

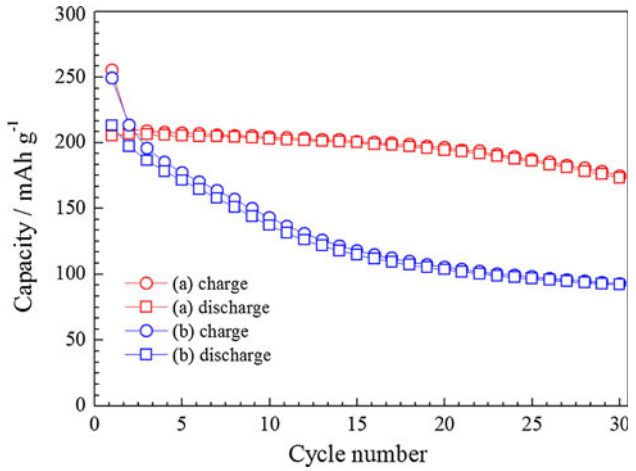

Fig. 10 Cycle performances at a rate of 1 C; **a** nano-sized MoO_2/C composite and **b** commercial MoO_2

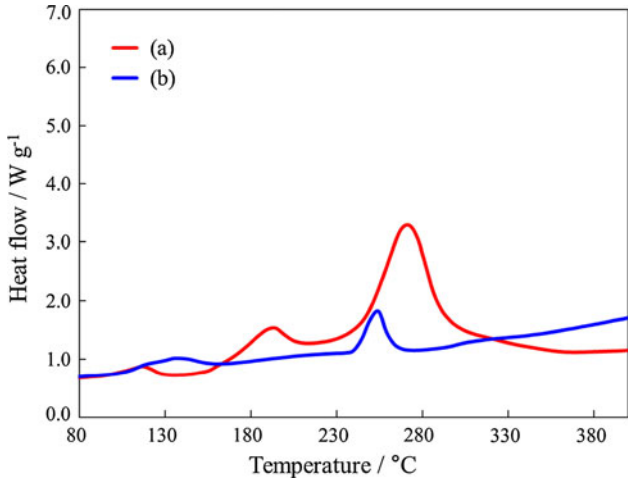

Fig. 11 DSC curves for discharged electrodes; **a** commercial natural graphite discharged to 0.01 V (vs. Li/Li^+) and **b** nano-sized MoO_2/C composite discharged to 0.8 V (vs. Li/Li^+)

maintained up to about 78 % at 5 C, while the capacity retention of the commercial MoO_2 is about 57 % at the same rate. The enhanced rate-capability of the nano-sized MoO_2/C is attributed to the short diffusion pathway for Li^+ insertion/extraction induced by the nano-sized primary particles and the effective dispersion of carbon in the MoO_2/C composite.

Figure 10 displays the cycle performances of nano-sized MoO_2/C and commercial MoO_2 at a rate of 1 C. Nano-sized MoO_2/C has good capacity retention, while commercial MoO_2 shows comparatively poor capacity retention during cycling. The poor cycle performance of commercial MoO_2 is caused by its large particle size of about 200–400 nm compared to the nano-sized MoO_2/C composite. It has been reported that the structural volume on changing from MoO_2 to $LiMoO_2$ increases by about 11 % [17]. The large volume change should introduce stress in the structure during cycling, so the cyclability will be decreased with degradation of the structure. The large volume change can be suppressed by decreasing the particle size, which therefore enhances the cycle performance.

The thermal stability of the MoO_2/C composite is shown in Fig. 11. The discharged MoO_2 materials show two exothermic peaks at around 130 and 255 °C. The former peak is related to the surface reaction of MoO_2, and the latter is related to the bulk reaction including structural destruction [31]. Nano-sized MoO_2/C exhibits better thermal stability than graphite negative electrodes from the view point of the on-set temperature and the total heat flow.

4 Conclusions

A spherical MoO_2/C composite with nano-sized primary particles was synthesized successfully by the spray pyrolysis technique. The sucrose additive assisted in reducing

the particle size, and also enhanced the electronic conductivity through the uniform dispersion of carbon. The nano-sized MoO_2/C showed an enhanced discharge capacity, rate-capability, and cycle performance compared to those of commercial MoO_2 powders. The improved electrochemical properties are attributed to the small primary particle size, which minimizes structural strain during cycling, the short diffusion pathways of the Li-ions, and the increased electronic conductivity due to the uniform carbon distribution in the composite. The MoO_2 material exhibits better thermal stability than commercial graphite materials. These results suggest that nano-sized MoO_2 has a potential as an anode material for lithium-ion batteries.

Acknowledgments This study was supported by the Energy Efficiency & Resources of the Korea Institute of Energy Technology Evaluation and Planning (KETEP) Grant funded by the Korea government Ministry of Knowledge Economy (Project No. 2011201010016B).

References

1. Terada N, Yanagi T, Arai S, Yoshikawa M, Ohta K, Nakajima N, Yanai A, Arai N (2001) J Power Sources 100:80–92
2. Armand M, Tarascon JM (2008) Nature 451:652–657
3. Bruce PG, Scrosati B, Tarascon JM (2008) Angew Chem Int Ed 47:2930–2946
4. Nishi Y (2001) J Power Sources 100:101–106
5. Li H, Huang X, Chen L (1999) Solid State Ion 123:189–197
6. Poizot P, Laruelle S, Grugeon S, Dupont L, Tarascon JM (2000) Nature 407:496–499
7. Poizot P, Laruelle S, Grugeon S, Dupont L, Tarascon JM (2001) J Power Sources 97–98:235–239
8. Yao XL, Xie S, Chen CH, Wang QS, Sun JH, Li YL, Lu SX (2005) Electrochim Acta 50:4076–4081
9. Ohzuku T, Ueda A, Yamamoto N (1995) J Electrochem Soc 142:1431–1435
10. Caleb AE, Oscar MF, Su H, Grant N (2012) J Mater Sci 47:2057–2071
11. Oh SW, Bang HJ, Bae YC, Sun YK (2007) J Power Sources 173:502–509
12. Rahman MM, Chou SL, Zhong C, Wang JZ, Wexler D, Liu HK (2010) Solid State Ion 180:1646–1651
13. Fu LJ, Zhang T, Cao Q, Zhang HP, Wu YP (2007) Electrochem Commun 9:2140–2144
14. Auborn JJ, Barberio YL (1987) J Electrochem Soc 134:638–641
15. Yang LC, Gao QS, Tang Y, Wu YP, Holze R (2008) J Power Sources 179:357–360
16. Shi Y, Guo B, Corr SA, Shi Q, Hu YS, Heier KR, Chen L, Seshadri R, Stucky GD (2009) Nano Lett 9:4215–4220
17. Dahn JR, McKinnon WR (1987) Solid State Ion 23:1–7
18. Andersson A, Hansen S (1988) Catal Lett 1:377–384
19. Sloczynski J (1995) J Solid State Chem 118:84–92
20. Doi T, Yahiro T, Okada S, Yamaki J (2008) Electrochim Acta 53:8064–8069
21. Song JH, Park HJ, Kim KJ, Jo YN, Kim JS, Jeong YU, Kim YJ (2010) J Power Sources 195:6157–6161
22. Inorganic Crystal Structure Database. Fach information szentrum (FIZ) Karlsruhe
23. Ku JH, Jung YS, Lee KT, Kim CH, Oh SM (2009) J Electrochem Soc 156:A688–A693
24. Yang LC, Gao QS, Zhang YH, Tang Y, We YP (2008) Electrochem Commun 10:118–122
25. Sun Y, Hu X, Luo W, Huang Y (2011) ACS Nano 9:7100–7107
26. Guo B, Fang X, Li B, Shi Y, Quyang C, Hu YS, Wang Z, Stucky GD, Chen L (2012) Chem Mater 24:457–463
27. Fang X, Guo B, Shi Y, Li B, Hua C, Yao C, Zhang Y, Hu YS, Wang Z, Stucky GD, Chen L (2012) Nanoscale 4:1541–1544
28. Borghols WJH, Wagemaker M, Lafont U, Kelder EM, Mulder FM (2009) J Am Chem Soc 131:17786–17792
29. Hirayama M, Kim K, Toujigamori T, Cho W, Kanno R (2011) Dalton Trans 40:2882–2887
30. Saravanan K, Ananthanarayanan K, Balaya P (2010) Energy Environ Sci 3:939–948
31. Yamaki J, Takatsuji H, Kawamura T, Egashira M (2002) Solid State Ion 148:241–245